Maternal Influenza A Virus Infection Induces Antiviral and Immune Dysregulation in the Placenta and Fetus Without Vertical Transmission

Orlando Cervantes[1,2], Hazel Huang[2], Sidney Sun[2], Briana Del Rosario[2], Hong Zhao[2], Amanda Li[2,3], Andrew Vo[2,5], Gygeria Manuel[2], Roslyn Van Abel[2], Jeff Munson[4], John Cornelius[2], Raj P. Kapur[6,7], Miranda Li[2,5], Edmunda Li[2], Hanning Li[2], Alexandra Christodoulou[8], Melissa Berg[8], Britni Curtis[8], Elizabeth Miller[8], Shannon Ruff[8], Brenna Menz[8], Solomon Wangari[8], Audrey Germond[8], Audrey Baldessari[8], Chris English[8], W. McIntyre Durning[8], Thomas B. Lewis[9], Megan N. Fredericks[9], Mara Maughan[9], Austyn Orvis[10], Michelle Coleman[10], Lakshmi Rajagopal[1,10,11], Deborah H. Fuller[8,9], Kristina M. Adams Waldorf[1,2,8,*]

[1] Department of Global Health, University of Washington, Seattle, WA, 98195

[2] Department of Obstetrics and Gynecology, University of Washington, Seattle, WA, 98109

[3] Case Western Reserve School of Medicine, Cincinnati, OH

[4] Department of Psychiatry, University of Washington, Seattle, WA, 98195

[5] School of Medicine, University of Washington, Seattle, WA, 98195

[6] Department of Lab Medicine and Pathology, University of Washington, Seattle, WA, 98195

[7] Department of Pathology, Seattle Children's Hospital, Seattle, WA,

[8] Washington National Primate Research Center, Seattle, WA, 98195

[9] Department of Microbiology, University of Washington, Seattle, WA 98195

[10] Center for Global Infectious Disease Research, Seattle Children's Research Institute, Seattle, WA

[11] Department of Pediatrics, University of Washington, Seattle, WA 98195

*Corresponding author: Dr. Kristina Adams Waldorf, 750 Republican St., Seattle, WA 98109; adamsk@uw.edu

Running Title: Placental-Fetal Immune Response to Influenza A Virus

Keywords: influenza, H1N1, placenta, interferon, fetus, pregnancy

Abstract Word Count (150 words): 148 words

Main Text Word Count (<4,000 words): 3,478

ABSTRACT

Influenza A virus (IAV) infection during pregnancy is associated with stillbirth and preterm birth, possibly by disrupting placental and fetal immunity. To investigate this, pregnant pigtail macaques were inoculated with IAV [A/California/07/2009 (H1N1)] and examined at necropsy 5 days post-infection (N=11) versus uninfected controls (N=16). Stillbirth occurred in 18% of infected pregnancies but not in controls. While vertical transmission was not observed, low levels of viral RNA were detected in two placentas. Maternal IAV infection was associated with increased placental IL-1β and IFN-β levels and an upregulated type I interferon and integrated stress transcriptional response. Fetuses exposed to IAV had greater frequencies of innate immune cells in lymph nodes and CD4+ T cells in lungs. These results suggest that placental and fetal immune environments undergo immune activation independent of the severity of maternal lung infection. Influenza vaccination during pregnancy may protect against potentially harmful effects on fetal development.

KEYWORDS: influenza A virus, H1N1, pregnancy, fetus, placenta, nonhuman primate, innate immunity

INTRODUCTION

Influenza A virus (IAV) infections remain a global public health threat, which is especially pronounced in vulnerable populations like pregnant women.[1,2] IAV is a negative-sense, single-stranded RNA virus composed of eight segments. Pandemics occur when reassortment of the viral segments occurs to produce new combinations of its surface glycoproteins, hemagglutinin (HA), and neuraminidase (NA). Epidemiologic evidence from several IAV pandemics (e.g., 1918, 1957, 1968, 2009) indicates that IAV infections in pregnancy impart a greater risk of maternal mortality and adverse pregnancy outcomes, such as stillbirth.[1-12] There may also be a long-term risk of neuropsychiatric disease in the children born to pregnant women infected with IAV or other infectious diseases, which has been reported in multiple populations.[13-20] Vaccination with the seasonal trivalent IAV vaccine has been associated with a reduced risk of stillbirth in some[21-25], but not all, studies.[9,26] Despite the public health recommendation for pregnant women to receive the seasonal IAV vaccine[27], only half of pregnant women in the U.S. typically receive the vaccination each year.[28]

Increasing vaccine skepticism since the COVID-19 pandemic requires a better public understanding of the importance of annual seasonal influenza vaccination to reduce the adverse impacts of IAV infections during pregnancy on placental and fetal health.[29,30] Reducing maternal mortality is an important benefit of vaccination, but in the absence of a pandemic, this rare outcome may not be perceived as a risk. A spectrum of adverse pregnancy and fetal outcomes has been reported in pregnant mice and rats[31-38], but these animal models are dissimilar to human pregnancy in many respects including a short gestation (3-5 weeks). Humans have a gestational period that is 8–10 times longer than these species, allowing for extended fetal brain development *in utero.* However, this long gestational period also increases the placenta and fetus' exposure to seasonal waves of IAV infection. Nonhuman primates (NHPs) share many similarities with human pregnancy, including a longer gestation, placental structure, and physiology of labor.[39,40] NHPs

are also frequently used in IAV disease modeling due to their similarities in human clinical and pathological features.[41,42] A few studies using pregnant NHPs have modeled IAV infection but were performed with the intent to understand complement activation and infant brain development in African green monkeys and rhesus macaques, respectively.[43,44] The broader impact of IAV infection during pregnancy on placental and fetal immunity and health was not characterized.

Our objective was to determine the impact of a maternal IAV infection with a 2009 pandemic strain, on innate and adaptive immune responses in the placenta and fetus of the pigtail macaque (*Macaca nemestrina*) model. There are comparatively few studies linking immune responses in the placenta with those in the fetus.[32,36,45,46] A secondary objective was to account for how differences in the severity of the maternal IAV infection might affect the placental immune response, as part of the larger nexus of crosstalk between the mother, placenta, and fetus during acute IAV infection.

RESULTS

Impact of Influenza A Viral Disease on Pregnancy Outcome and Lung and Placental Histopathology

Eleven pregnant pigtail macaques were inoculated with an IAV H1N1 2009 pandemic strain (A/CA/07/2009) in the third trimester (FLU cohort) using a combination of intranasal, intratracheal, intraocular, and intraoral routes with 7.4×10^6 plaque-forming units (PFU). Results were compared to 16 historical control uninfected pregnant pigtail macaques (CTRL cohort, Table S1). Five days after inoculation, Cesarean section and necropsies of the dam and fetus were performed. Stillbirth occurred in two of the eleven FLU pregnancies (18%, FLU7 and FLU9), but in no CTRL animals. Clinical signs of maternal illness were documented using daily clinical scores and vital signs taken at the time of sedations: before inoculation, 1- and 3-days post-inoculation (dpi), and on 5 dpi, the

experimental endpoint (Table 1). Coughing, wheezing, increased respiratory effort, nasal discharge, and decreased appetite were common symptoms in 7 of 11 FLU animals (64%), while the remaining four did not show clinical symptoms. Animals that exhibited the most severe disease based on clinical scores were FLU8 and FLU9; of these animals, FLU9 experienced a stillbirth. Clinical scores were highest between day 3 and day 5 post-inoculation. Uninfected CTRL animals did not show signs of respiratory disease.

Histopathology of the maternal lungs and placentas was evaluated to determine if IAV inoculation induced influenza-associated pathology in either organ (Fig. 1, Table S2). Lung histopathology revealed pneumonia in all cases, including the two cases with stillbirth; one dam experiencing a stillbirth had mild, multifocal pneumonia (FLU7), and the other had severe pneumonia with pleural effusion and hilar lymphadenopathy (FLU9). Of the CTRL animals with histopathology data available, none had pulmonary inflammation. Most placentas from FLU animals had evidence of either placental infarction (coagulative villous necrosis), neutrophilic (necrotizing) villitis, or both (8/11, 73%; Fig. 1B-C, Table S2). Infarction or active inflammation was observed less frequently in the CTRL placentas (5/16, 31%). None of the placentas demonstrated active inflammation of the chorioamniotic membranes. Placental histopathology in the two stillbirth cases (FLU7, FLU9) overlapped with that observed in other IAV-infected animals, and some CTRL animals.

110 Figure 1. Placental histopathology

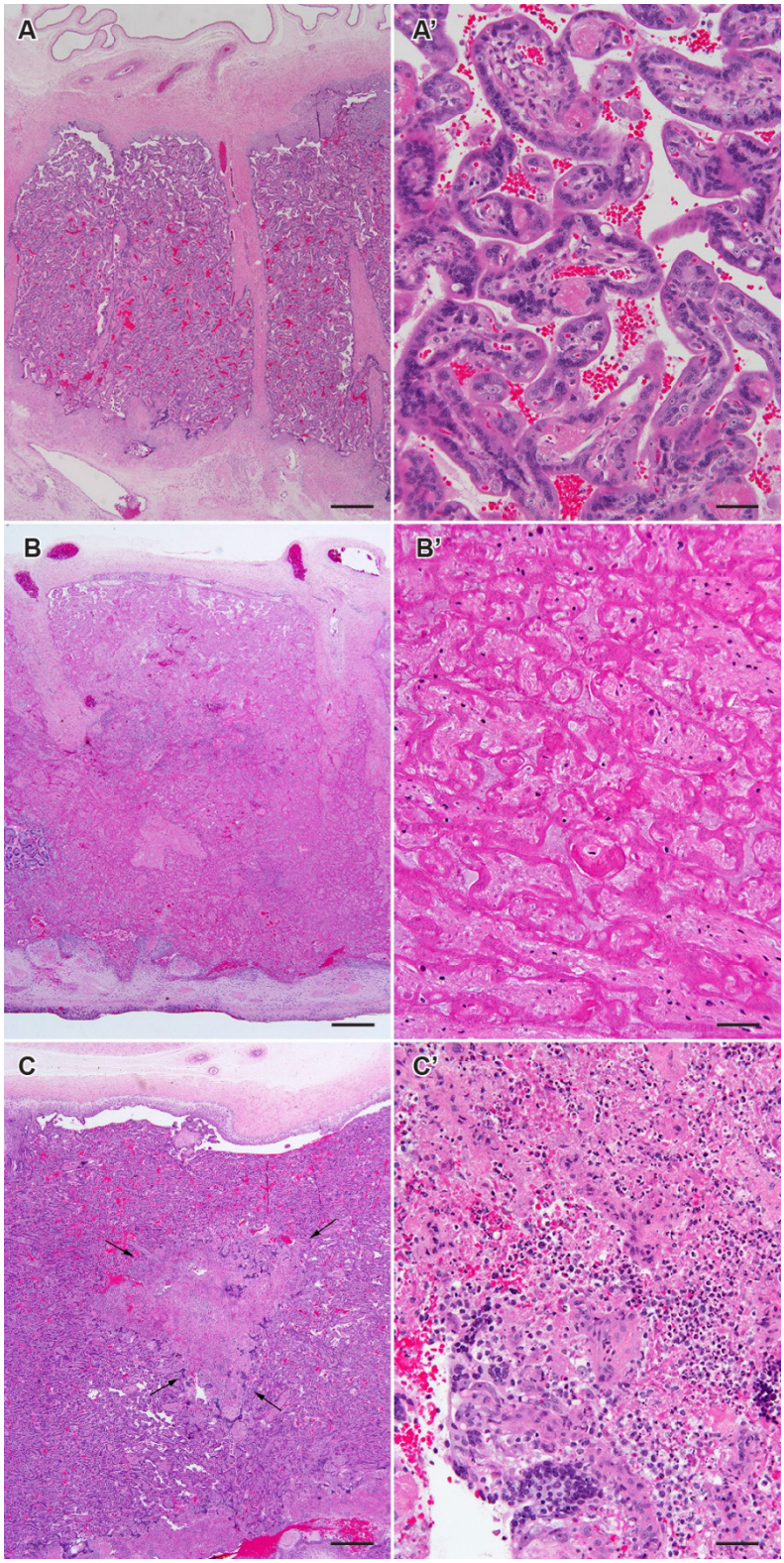

Each pair of images shows a low-magnification image of the placental disc (fetal surface toward the top) on the left and a higher-magnification image of villous tissue on the right. (A, A') Normal placental anatomy from a control animal showing no inflammation or necrosis. (B, B') A focus of subacute infarction with coagulative necrosis and no active inflammation is shown from a representative animal in the FLU cohort. (C, C') A focus of necrotizing villitis (highlighted by arrows) with neutrophilic inflammation and villous necrosis is shown from a representative animal in the FLU cohort.

131 *IAV H1N1 vRNA in Lung, Placenta, and Fetus*

132 RT-qPCR was performed to measure IAV viral RNA (vRNA) in the maternal lungs, placenta, and
133 fetal organs (Table 1). At 5 dpi, all FLU animals had high levels of IAV vRNA in their lungs ranging
134 from 2,220 copies per milligram to more than 6 million copies per milligram. One exception was
135 FLU10, which had an almost undetectable lung viral load (3 copies/mg). IAV vRNA was detected
136 in the placental chorionic villous tissue of only two cases (2/11; 18%), both with a low copy number
137 in the placenta (FLU1 and FLU9; Table 1). Of these, FLU9 additionally experienced stillbirth. Fetal
138 tissue samples from the brain, brainstem, spinal cord, meninges, heart, lungs, liver, spleen, and
139 thymus were negative for IAV H1N1 vRNA across the entire FLU cohort (Table S3). Overall, the
140 maternal lung was characterized by a wide distribution of IAV viral load, infrequent detection of
141 IAV vRNA in placental tissues, and no evidence for congenital infection.

142 *Cytokine Concentrations in the Placental Disc and Amniotic Fluid*

143 Cytokine responses in the placental disc and amniotic fluid were evaluated to determine if there
144 was a correlation between maternal IAV infection status, viral load, or stillbirth. Chorionic villous
145 tissue from the placenta disc of FLU animals had significantly greater concentrations of some
146 inflammatory and antiviral cytokines than CTRL placentas, including IL-1β, IL-18, IFN-β, and GM-
147 CSF (all $p \leq 0.03$, Fig. 2). The highest concentrations of IFN-α, IFN-β, IL-6, TNF, and GM-CSF
148 within the FLU cohort were observed in both placentas with low IAV viral load, of which one was
149 a stillbirth case; however, the second stillbirth case had low cytokine concentrations. Several
150 cytokines with low expression (IL-2, IL-10, IL-12p70, IL-13, IL-17A, and IL-23) were significantly
151 higher in the CTRL versus FLU cohort (Fig. S1). However, in many cases, these cytokine values
152 fell below the working range of the Luminex assay.

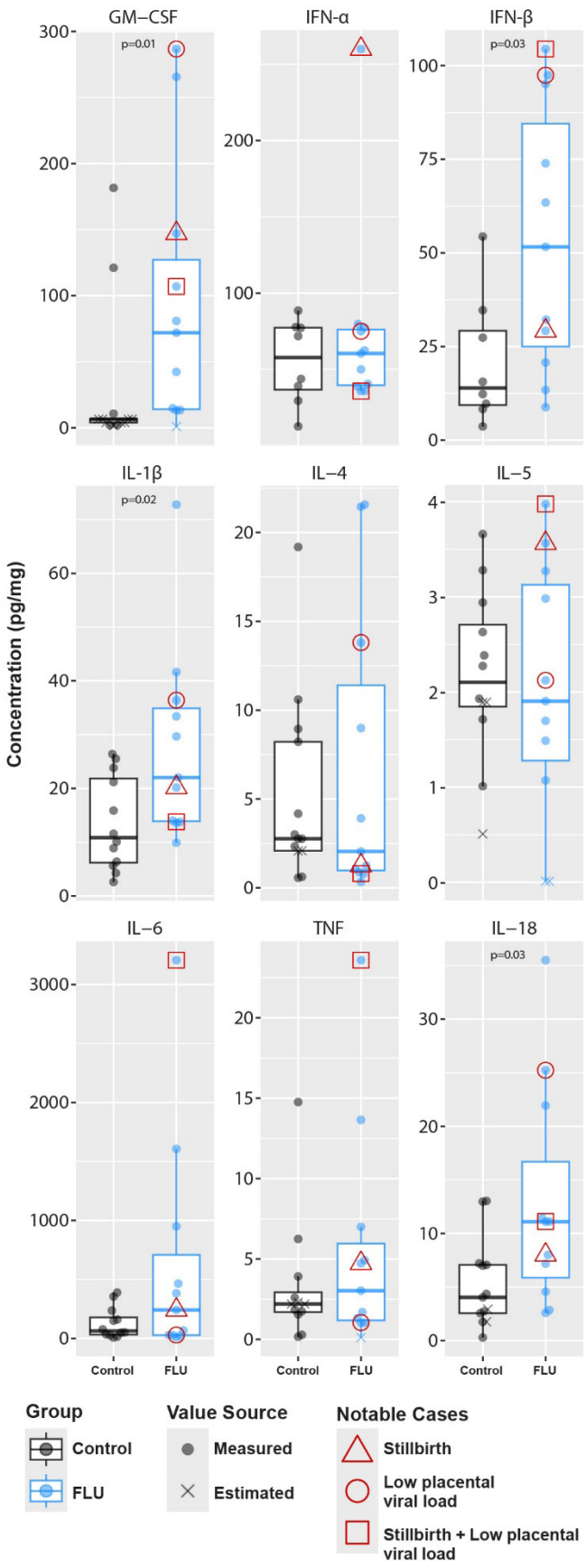

Figure 2. Cytokine concentrations in the placental disc.

Each panel shows the concentration of a cytokine quantified by multiplex Luminex assay in chorionic villous tissue from the FLU (blue) and CTRL (black) cohorts. Values are either measured (dots) or estimated (x's) by extrapolation of the standard curve. The thick line indicates the median, and the bounding box indicates the 1st and 3rd quartiles. Red triangles marks samples from animals that experienced a stillbirth. A red circle marks samples from animals that had a low placental viral load. A red square marks samples from animals that experienced a stillbirth and had low placental viral load. The p-value for CTRL versus FLU cohorts is indicated at the top of each panel if less than 0.05.

174 In contrast to chorionic villous tissue, several cytokines in the amniotic fluid were significantly
175 higher in the CTRL versus FLU cohort (GM-CSF, IFN-β, IFN-γ, IL-1β, IL-4, IL-5, IL-13, IL-17A,
176 and IL-23; all $p<0.05$). In most cases, the concentration of the cytokines in both cohorts was very
177 low (Fig. S2). These results indicate that perturbations in cytokines associated with maternal IAV
178 infection were compartment-specific, and elevated cytokines in the chorionic villous tissue were
179 not transported into the amniotic fluid compartment.

180 *Immune Cell Frequencies in the Placenta, Fetal Blood and Organs*

181 To determine if a maternal IAV H1N1 infection was associated with changes in the innate and
182 adaptive immune cell composition of the placental disc, we performed an immunophenotyping
183 assay using flow cytometry. The frequency of classical monocytes among live leukocytes was
184 significantly decreased in the placental disc of the FLU versus CTRL cohort ($p=0.004$, Fig. 3).
185 Immune cell frequencies between the FLU and CTRL cohorts were variable in the chorionic villous
186 tissue, making it challenging to ascertain significant differences between the two groups with
187 modest group sizes. There was no relationship between stillbirth and the frequency of immune
188 cell populations in the placenta.

Figure 3. Immunophenotyping of the placental disc by flow cytometry

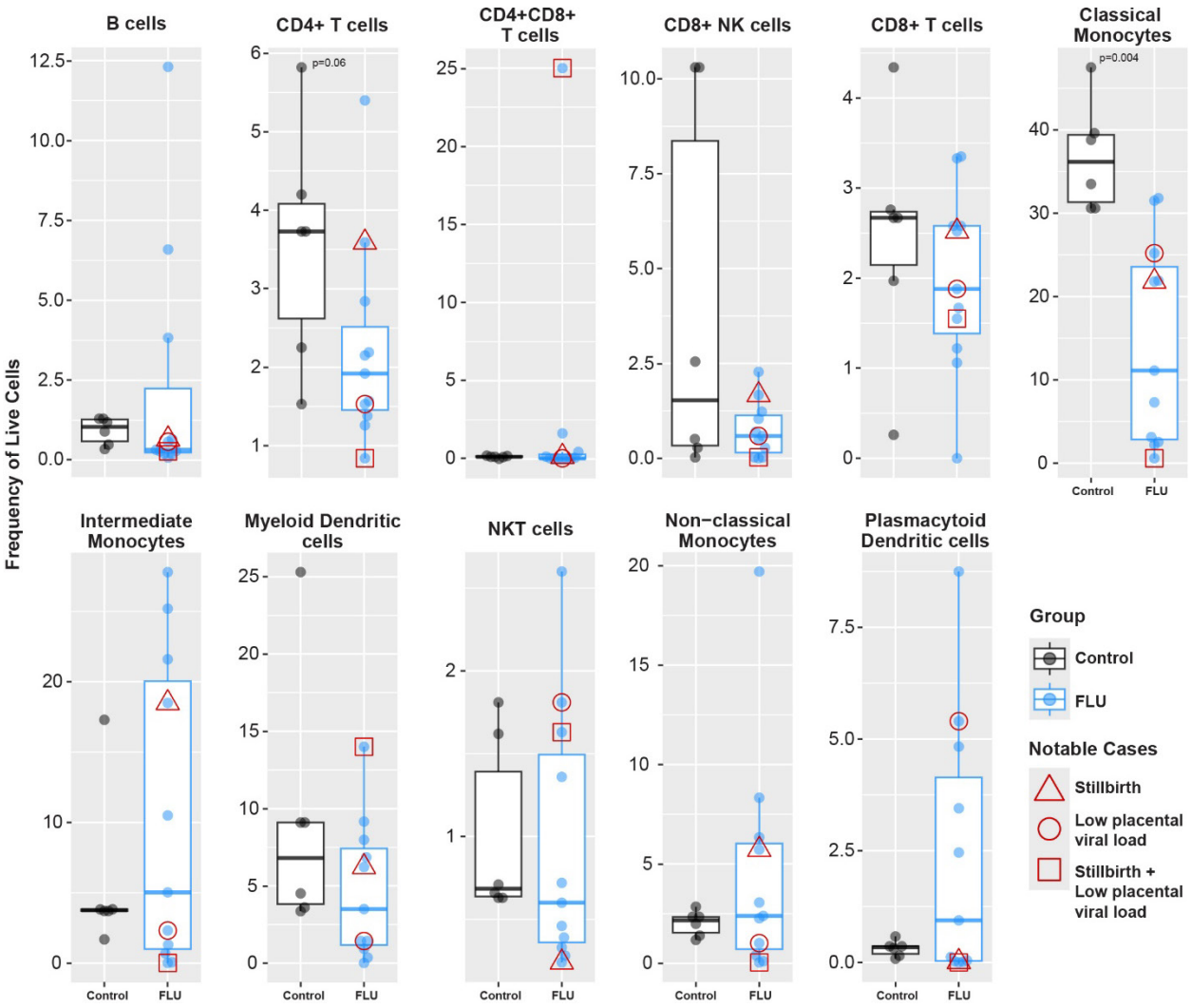

Each panel shows the frequency of the defined cell population as a percentage of live cells, in chorionic villous tissue of the FLU (blue) and CTRL (black) cohorts. The thick line indicates the median, and the bounding box indicates the 1st and 3rd quartiles. A red triangle marks samples from animals that experienced stillbirth. A red circle marks samples from animals that had a low placental viral load. A red square marks samples from animals that experienced a stillbirth and had low placental viral load. The p-value for CTRL versus FLU cohorts is indicated at the top of each panel if less than 0.05.

198 In fetal organs, there was a coordinated perturbation of innate immune cells and T cells in the
199 FLU versus CTRL cohorts. In the fetal lung, the frequencies of intermediate monocytes, non-
200 classical monocytes, plasmacytoid dendritic cells, and CD4+ T cells were significantly higher in
201 the FLU cohort compared to the CTRL cohort ($p \leq 0.04$, Fig. S3). A similar pattern was evident in
202 the fetal mesenteric lymph nodes, with a significantly higher frequency of intermediate monocytes
203 ($p=0.02$), and observably higher frequencies of NKT cells, non-classical monocytes, and
204 plasmacytoid dendritic cells in the FLU versus CTRL cohort ($p=0.06$, Fig. S4). In fetal whole blood,
205 there was a significantly higher frequency of NKT cells in the FLU cohort ($p=0.03$, Fig. S5). These
206 differences suggest that maternal IAV H1N1 infection perturbs populations of fetal innate and
207 adaptive immune cells in organs, lymphoid compartments, and blood even without evidence of
208 vertical transmission.

209 *Placental Transcriptional Profile*

210 To determine if a maternal IAV infection altered the transcriptional signature in the placental disc,
211 we performed total RNA-Seq on chorionic villous tissues and validated our results by direct gene
212 counting using a Nanostring nCounter assay. A multidimensional scaling plot of the normalized
213 RNA-Seq gene counts demonstrated a clear division between the two cohorts (Fig. 4A; CTRL,
214 blue dots) and FLU (red symbols). In the placental chorionic villous tissue, 185 genes were
215 upregulated, and 178 genes were downregulated relative to the gene expression of the CTRL
216 group (≥ or ≤ 1.5-fold, $p<0.05$; Fig. 4B). Inspection of the upregulated genes revealed a striking
217 upregulation of interferon (IFN)-stimulated genes (ISGs) including *IFIT3, MX1*, and *OAS2* in
218 placentas from FLU animals relative to CTRL placentas. A Gene Set Enrichment Analysis (GSEA)
219 revealed multiple significant, positively enriched pathways related to the type I IFN response and
220 the negative regulation of viral processes such as genome replication and viral entry in FLU
221 versus CTRL animals (Fig. 4C). Digital gene counting using a 770-plex Nanostring nCounter
222 panel supported these results with a similar striking upregulation of ISGs (Fig. S6), and strong

223 correlation with total RNA-Seq gene counts in both the FLU and CTRL groups (Fig. 4D; r=0.8,

224 $p<2.2x10^{-16}$ for both).

225 Figure 4. Total RNA-Seq of the placental disc from FLU and CTRL animals.

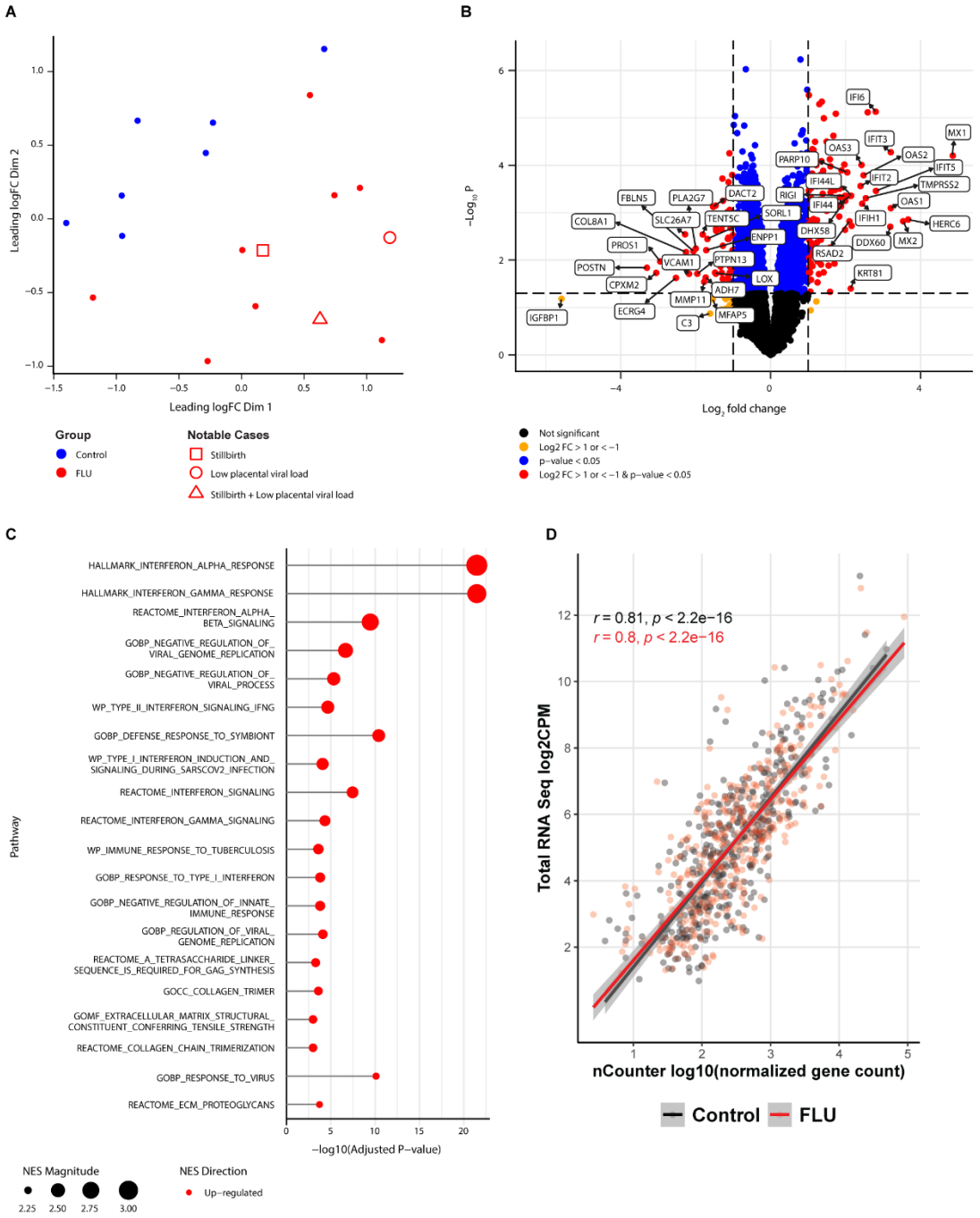

226

227 (A) Multidimensional scaling (MDS) was performed on normalized log-transformed gene counts
228 using the Euclidean distance. Each point represents an individual sample, and the distance
229 between points reflects the relative similarity of their global expression profiles. Samples are
230 colored according to experimental group (FLU: red; CTRL: blue). Symbols denoted the following:
231 an open red circle for low placental IAV vRNA, an open red square for a stillbirth with undetectable
232 vRNA, and an open red triangle for a stillbirth with low vRNA. (B) A volcano scatter plot illustrates
233 the relationship between the log2 fold change of gene expression (x-axis) and statistical
234 significance [-log10 (p-value), y-axis] of differentially expressed genes between the FLU and
235 CTRL cohorts. Dot colors indicated significance and magnitude: red for genes with significant log2
236 fold change ≥1 or ≤–1; blue for genes with |log2 fold change| <1 but $p<0.05$; gold for non-
237 significant genes with |log2 fold change| ≥1; and black for non-significant genes with |log2 fold
238 change| <1. (C) A Gene Set Enrichment Analysis of significant Gene Ontology (GO) terms in FLU
239 versus CTRL placentas is shown ($p<0.05$). Colored dots indicate the Normalized Enrichment
240 Score (NES), which evaluates the degree to which a set of genes in a GO category is over-
241 represented in a ranked gene list. The FDR, or false discovery rate, is a statistical method used
242 to correct for multiple testing when analyzing many GO terms simultaneously. (D) This dot plot
243 illustrates the correlation between the placental log2-transformed gene counts per million
244 obtained from total RNA-Seq and the log10-transformed gene counts from the Nanostring
245 nCounter assay. Each dot represents a mean value of a gene count from either the FLU (red) or
246 CTRL (black) group, which has both nCounter and RNA-Seq data. A Pearson correlation test was
247 performed, and the r coefficient and p-value for each group are noted in the upper left-hand corner
248 of the plot. The line of best fit with standard error is shown.

249 Next, we evaluated whether the viral infection in the mother's lungs or cytokines produced in the
250 lung or placenta might be driving these findings. We performed unsupervised hierarchical
251 clustering of the placenta RNA-Seq data and initially ordered the heatmap according to the

maternal lung viral load or Type I IFN cytokine concentrations in the lung and placenta (Fig. 5A). No clear pattern in the placental transcriptional response emerged regardless of how the heatmap was ordered, whether it be by lung viral load, IFN-α (lung, placental disc) or IFN-β (placental disc) concentrations. No correlation was observed between placental RNA-Seq gene counts and placental viral load, which was undetectable in all but two cases.

Hierarchical clustering yielded two distinct clusters of differentially expressed genes: cluster 1 (downregulated genes, FLU vs. CTRL; Fig. 5B) and cluster 2 (upregulated genes, FLU vs. CTRL; Fig. 5C). Overrepresentation Analysis (ORA) was performed to identify Gene Ontology (GO) terms enriched in both clusters. No significant GO terms were identified in cluster 1. However, inspection of genes in cluster 1 revealed downregulation in the FLU group of multiple genes involved in ubiquitination, proteasome function, unfolded protein response, metabolism, and cell cycle/DNA repair (Fig. 5B). To determine if this profile might reflect induction of a viral-associated integrated stress response (ISR), we analyzed expression of two key genes in the pathway: *EIF2AK2* (ISR activator) and *ATF4* (ISR effector). Of these genes, *EIF2AK2* expression was significantly upregulated in the placenta [log2 fold change=1.24, $p<0.05$; Fig. 5B]. In cluster 2, significantly enriched GO terms in the FLU cohort were related to type I and II interferon signaling, viral genome regulation, and antiviral defense processes that featured ISG genes (Fig. 5C; Fig. S7). A notable outlier was FLU11, which had a transcriptional profile more similar to CTRL animals. Placental transcriptomics of FLU3 and FLU4 were intermediate between the FLU and CTRL cohorts. Collectively, transcriptional analysis of the placental chorionic villous tissue from FLU animals revealed a striking upregulation of antiviral innate immune genes and downregulation of critical cellular functions (cell cycle, metabolism, ubiquitination) consistent with an antiviral and ISR response, regardless of the severity of disease in the maternal lung.

Figure 5. RNA-Seq analysis of placental chorionic villous tissue in FLU and CTRL groups

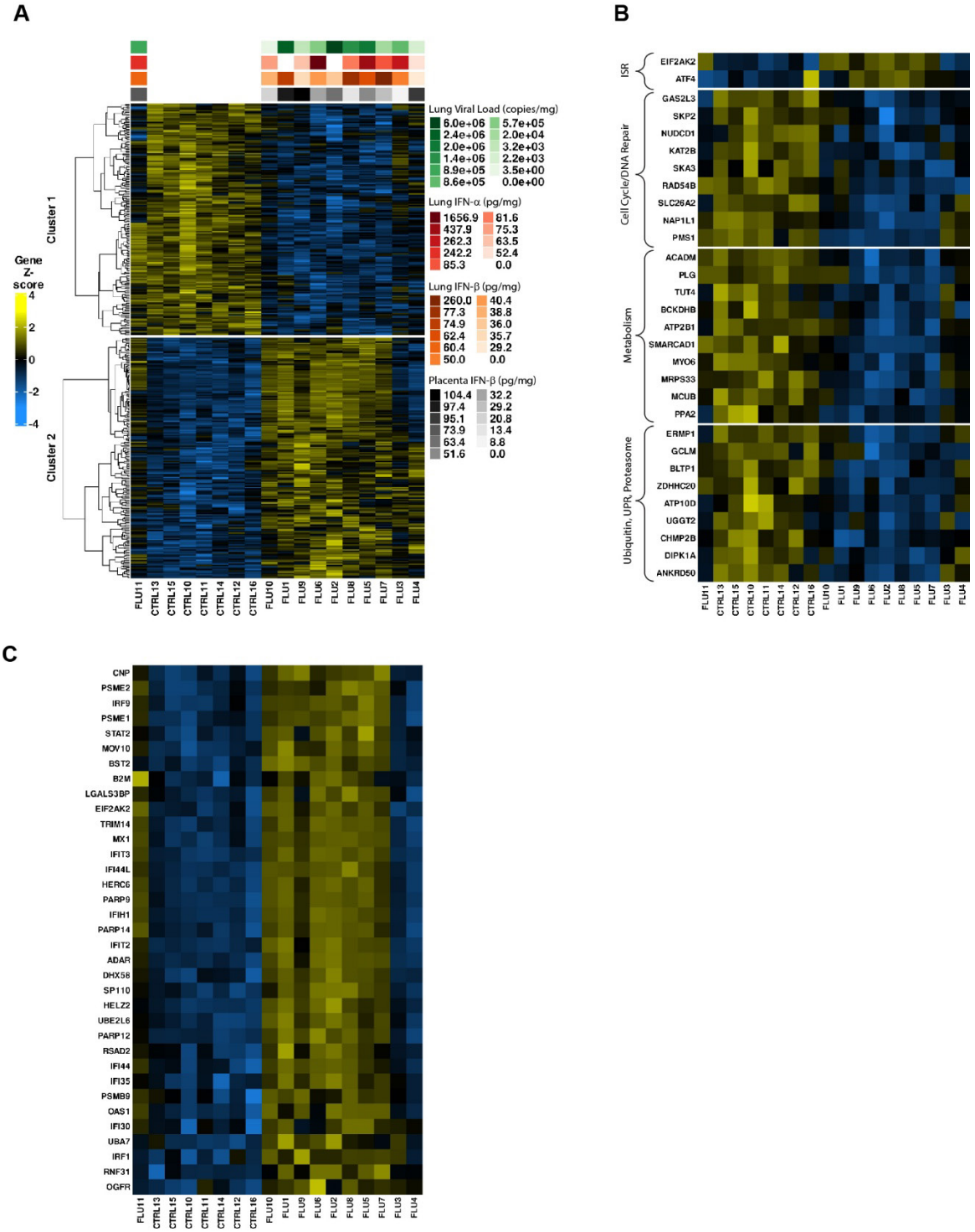

Heatmaps are shown of normalized counts from the placental total RNA-Seq data from the FLU and CTRL cohorts. Each column represents an individual placental sample, and each row

279 represents an individual gene. The yellow-blue color intensity indicates the gene z-score which
280 was calculated based on the mean expression level of all animals for each gene. (A) An
281 unsupervised hierarchical clustering analysis was performed on the top 500 differentially
282 expressed genes in the placentas of the FLU cohort using the Euclidean distance metric and
283 Ward's method. The relative quantity of maternal lung viral load in the IAV-infected group is
284 indicated by the green color gradient. Lung IFN-α and IFN-β, and placenta IFN-β concentrations
285 are indicated by red, orange, and gray color gradients, respectively. (B) Cluster 1 genes from
286 panel A are shown, which have functions impacted by the viral-associated ISR, such as cell
287 cycle/DNA repair, metabolism, ubiquitination, unfolded protein response (UPR), and proteasome
288 activity. The viral-associated ISR activator (*EIF2AK2*) and mediator (*ATF4*) are shown at the top.
289 (C) An over-representation analysis (ORA) was performed on cluster 2 genes from panel A. Rows
290 are genes in the Molecular Signatures Database Gene Set: Hallmark Interferon Alpha Response.

291 **DISCUSSION**

292 Our results indicate that IAV infection in pregnant NHPs induces a placental stress response and
293 alters the immune environment in both the placenta and fetus, even in the absence of detectable
294 viral infection in these compartments. Interestingly, placental injury and abnormal gene
295 expression was observed among all IAV-infected animals despite significant variability in viral
296 load and type I interferon concentrations in the maternal lungs. To our knowledge, this is the first
297 demonstration that maternal IAV lung infection, independent of disease severity, drives significant
298 alterations in placental gene expression, emphasizing the placenta's function as an
299 immunologically responsive organ to maternal systemic inflammation. This key finding suggests
300 that pregnant women with even a mild course of IAV disease at the time of birth are as vulnerable
301 to placental and fetal innate immune dysregulation as those with severe infection.

302 While direct placental infection and vertical transmission of IAV is rare, our data show that
303 maternal infection can disrupt the fetal innate and adaptive immune environment. This cascading
304 series of linked biological events, beginning in the mother's lungs and moving to the placenta,
305 demonstrates how a pulmonary viral infection can influence fetal development and potentially
306 prime the fetus for long-term health consequences. Dysregulation of the immune environment in
307 the fetus may be subtle but could underlie the increased lifetime risk of neuropsychiatric
308 conditions observed in children exposed to influenza and other infections *in utero*.[13,14,19,20,47,48] We
309 recently reported granular cytoplasmic inclusions in astrocytes within the deep white matter of
310 fetal pigtail macaques, a pathological finding that was more frequent in fetuses exposed to a
311 maternal IAV infection.[49] The impact of perturbations in fetal immunity and subtle changes in the
312 fetal brain associated with congenital infections are unknown, but it is a concerning potential risk
313 factor for abnormal neurodevelopment and a spectrum of neuropsychiatric diseases.

314 A defining feature of our study was the identification of a robust type I interferon (IFN-β) response
315 and inflammasome activation (IL-1β, IL-18) in the placenta. IAV is known to upregulate type I IFNs

316 in the lungs, but in the absence of placental infection, it has not been clear the degree to which
317 the virus in the lungs might induce an antiviral response in the placenta. Many of the upregulated
318 genes we observed are known to restrict IAV infection by sensing viral RNA (*DDX58*), restricting
319 viral entry (*MX1*) or replication (e.g., *IFIT2*, *EIF2AK2*), and destroying viral RNA (e.g., *OAS2,*
320 *OAS3*). Limited evidence suggests that IAV can replicate in the placenta and transfer to the fetus,
321 and documentation of this phenomenon or transplacental passage has been rare.[50,51] The
322 placenta's robust antiviral innate immune defense likely comes at a cost: type I IFNs and
323 inflammasome activation can lead to tissue injury, a known risk factor for stillbirth and preterm
324 birth.[52,53] The degree to which the placenta can balance the competing needs of viral clearance
325 without inciting tissue injury likely holds the key to preventing stillbirth.

326 NHPs in this study were not previously vaccinated against IAV and had no prior IAV infection. In
327 an IAV-naïve host, maternal CD8+ T cell activation is expected to begin within a few days, peak
328 in the draining lymph nodes between days 3-5, and become detectable by days 5-7, where they
329 aid in viral clearance.[54] Viral control in this early stage was likely exclusively a product of the
330 antiviral innate immune response in the maternal lung, which may have indirectly activated similar
331 responses in peripheral organs, including the placenta. In parallel, the viral-associated ISR may
332 equally impair critical cellular function in the placenta like DNA replication, enzymatic reactions,
333 and management of accumulating unfolded and misfolded proteins. An ISR is triggered by the
334 cell in response to a variety of stressors, including viral infections, and has significant interaction
335 with innate immune signaling pathways.[55,56] A critical requirement to activate the ISR, regardless
336 of the type of stressor, is the phosphorylation of eukaryotic translation initiation factor-2α
337 (EIF2α) by a variety of kinases, one of which is EIF2αK2.[57] Upregulation of *EIF2AK2*, and
338 downregulation of critical cell functions impacted by ISR (ubiquitination, metabolism, cell cycle,
339 DNA repair) provides strong evidence that the ISR pathway is induced in the placenta during a
340 maternal IAV infection. The virus exploits ISR to prevent the host cell from expending energy on

anything other than viral replication. If these cellular functions cannot recover, apoptosis can be initiated by *ATF4* and may disrupt placental functioning; increased expression of ATF4 was seen in some, but not all FLU cases.[56] The combination of a Type I IFN response and the viral-associated ISR may underlie stillbirth risk in pregnant women infected with IAV.

The primary strength of our study lies in the translational nature of the NHP model, which closely recapitulates human pregnancy, allowing one to model an IAV infection in the context of pregnancy. NHPs are highly similar to humans in their genetics, anatomy, physiology, immune responses, and pregnancies.[39] Macaques have a long gestational period and similar placental architecture to humans. Another strength of the pregnant NHP model of IAV infection is the ability to study antiviral immune responses at a defined time after infection onset, which is not possible during human pregnancy. Further, this study was deliberately conducted in the third trimester of pregnancy, a time when pregnant women experience the greatest maternal morbidity and mortality.[58,59] These features of the pregnant NHP model of IAV infection demonstrate the translational relevance of this model and the marked impact of our findings.

A spectrum of pathology was observed in the FLU placentas, which was also observed in some normal human pregnancies[47,48] However, two stillbirths occurred in our study, which were associated with placental infarctions in one case, and neutrophilic villitis, necrosis, and fibrin deposition in the other. In human cases of stillbirth, it is routine to extensively sample the placenta to survey histopathology across the entire disc. Greater sampling of the placenta in our NHP cohorts for histopathological analysis would have helped render a clearer determination of the underlying cause of the two stillbirths. Another important limitation was that we did not study endpoints earlier or later than five days post-infection, preventing assessment of the trajectory of the antiviral response in the maternal lungs and placenta.

Pandemic preparedness is critical to ensure that pregnant women have access to IAV vaccines, and for preventing stillbirth and maternal mortality. Currently, there is concern that a highly

366 pathogenic IAV H5N1 strain may spill over into humans and become readily transmissible. IAV
367 H5N1 and other highly pathogenic strains have been associated with excess mortality and
368 stillbirth in human cohorts.[60,61] Our results suggest that a pandemic IAV strain infecting the
369 maternal lungs adversely affects placental and, ultimately, fetal health. This data provides new
370 evidence supporting IAV vaccination in pregnancy as an actionable step to prevent not only
371 maternal mortality, but also viral injury to the placenta, disordered immune responses in the fetus,
372 and stillbirth.

373

374

375 **ONLINE METHODS**

376 *Research Animals and Ethics Statement*

377 All animal experiments used in this study were approved by the University of Washington
378 Institutional Animal Care and Use Committee (protocol# 4165-03, last approved 07/22/2025), and
379 in compliance with the U.S. Department of Health and Human Services Guide for the Care and
380 Use of Laboratory Animals and Animal Welfare Act. All animal experiments were performed at
381 the Washington National Primate Research Center (WaNPRC).

382 *Study Design*

383 Two groups of female pigtail macaques *(Macaca nemestrina*) were inoculated using a
384 combination of intranasal, intratracheal, intraocular, and intraoral routes with $10^{7.4}$ PFU of IAV
385 [A/California/07/2009 (H1N1)], reflecting a dose previously used in a study of cynomolgus
386 macaques (*Macaca fascicularis*).[62] Experimental groups consisted of IAV H1N1-infected pregnant
387 (N=11) and uninfected pregnant controls (N=18; Table S1). IAV inoculation occurred in the early
388 third trimester to model the time in pregnancy when IAV H1N1 infections are thought to produce

389 the greatest maternal lung disease and pregnancy complications.[11,12] Uninfected controls in this
390 study consisted of pregnant adult pigtail macaques used in prior published studies.[63,64]

391 Macaques inoculated with IAV were observed daily for clinical symptoms of influenza disease,
392 which were scored on a 3-point scale to reflect responsiveness of the animal, nasal or ocular
393 discharge, cough, respiratory effort, food consumption, and fecal consistency; higher scores
394 reflected disease, with a 0 in each category indicating a normal assessment. We chose a
395 predefined study endpoint of 5 days post-inoculation (dpi) to capture immune responses near the
396 peak of disease.[35,36] A Cesarean section was performed at the endpoint, and placentas were
397 extracted to sample chorionic villous tissue. The dam was euthanized using a barbiturate
398 overdose while under anesthesia. The fetus was euthanized using a barbiturate overdose,
399 followed by exsanguination. These methods are approved by the 2007 American Veterinary
400 Medical Association Guidelines on Euthanasia. Necropsies were performed on both the dam and
401 the fetus to obtain samples for transcriptomics, immune assays, and histopathology. Random
402 sections of the placental membrane, chorionic disc, and umbilical cord were evaluated for
403 pathology.

404 *H1N1 Virus Cultivation and Quantification*

405 We used an IAV strain [A/California/07/2009 H1N1 influenza virus (CA09)] that was obtained from
406 the World Reference Center for Emerging Viruses and Arboviruses at the University of Texas
407 Medical Branch at Galveston. Before culturing the virus, Madin-Darby canine kidney (MDCK) cells
408 (ATCC, Manassas, Virginia, US) were cultured in Dulbecco's modified Eagle's medium (DMEM)
409 supplemented with 10% fetal bovine serum (FBS), 25 mM HEPES, 100 U/mL penicillin, and 100
410 µg/mL streptomycin. Cells were incubated at 37°C and 5% CO_2 and confirmed to be free of
411 mycoplasma with the MycoAlert™ mycoplasma detection kit (Lonza, LT07-318) before use for
412 virus cultivation. Sub-confluent monolayers of MDCK cells in T150 flasks were washed with PBS
413 and infected at a multiplicity of infection (MOI) of 0.5 (5 mL serum-free MEM) at 37°C and 5%

414 CO_2. After 1 hour, the media was removed, cells were washed with 1X PBS, and the media was
415 replaced. The supernatant was harvested after 36 hours and centrifuged at room temperature to
416 remove cellular debris (1800 rpm for 5 minutes, followed by 3000 rpm for 10 minutes). Virus stock
417 was frozen at −80°C. The viral titer of each stock was quantified using a TCID50 assay with
418 hemagglutination readout and converted to PFU/mL.[65] To transform TCID50/mL into PFU/ml,
419 TCID50/mL was multiplied by 0.7. Reagents were obtained from Thermo Fisher Scientific unless
420 otherwise stated (Waltham, MA).

421 *RNA Isolation and Reverse Transcription Quantitative Polymerase Chain Reaction (RT-qPCR)*

422 Tissue samples were kept in RNAlater™ Stabilization Solution (#15596018, Thermo Fisher
423 Scientific) prior to homogenization in Precellys homogenizing tubes (#1011152, Cayman
424 Chemical, Ann Arbor, MI, USA) with the Precellys Evolution machine (Bertin Technologies,
425 Montigny-le-Bretonneux, France). RNA was extracted from homogenates using the RNeasy Mini
426 Kit (Qiagen, #74106). RNA was quantified using the NanoDrop™ 2000 spectrophotometer
427 (Thermo Scientific, #ND-2000) and the Qubit 4 fluorometer (Invitrogen, #Q33238). RNA quality
428 was evaluated by measuring the RNA integrity number (RIN) with the 4200 Tapestation System
429 (Agilent, #G2991BA).

430 To quantify IAV vRNA levels from different sample origins, we used reverse transcription
431 quantitative polymerase chain reaction (RT-qPCR) and a WHO-approved primer/probe set.[66]
432 cDNA was generated from RNA isolates using an iScript™ Select cDNA synthesis kit (Bio-Rad,
433 #1708897) using H1N1 HA-specific forward primer following manufacturer's instructions. qPCR
434 was done with H1N1 HA-specific primers and probes (Forward: GGGTAGCCCCATTGCAT;
435 Reverse: AGAGTGATTCACACTCTGGATTTC; Probe: 5`-[FAM]
436 TGGGTAAATGTAACATTGCTGGCTGG [TAMRA]-3`) using the Taqman Fast Advanced Master
437 Mix (#444964, Thermo Fisher Scientific) and a QuantStudio 3 machine (#A28132, Thermo Fisher

438 Scientific) following manufacturer instructions. Samples were run in triplicate. Positive results
439 were defined as any sample with an average Ct value less than 38 cycles.

440 *Cytokine Quantification*

441 ProcartaPlex™ NHP multiplex kits were used to quantify cytokines from lysates or fluids (Thermo
442 Fisher Scientific). Tissue lysis and homogenization were performed using an Invitrogen™
443 ProcartaPlex™ Cell Lysis Buffer (#EPX-99999-000, Thermo Fisher Scientific) with the addition of
444 a protease inhibitor cocktail (Fisher Scientific, #PI78430) using the Precellys Evolution system,
445 as previously described. Type I Interferons [IFN; IFN-alpha (IFNα) and IFN-beta (IFNβ)] were
446 quantified using the Cynomolgus IFN-beta and Cynomolgus/Rhesus IFN-alpha ELISA kits
447 (#46415-1 and #46100-1, respectively; PBL Biosciences, Menlo Park, CA, USA). All protocols
448 followed the manufacturer's guidelines.

449 *Immunophenotyping (IMP)*

450 Immunophenotyping by flow cytometry was performed to determine the frequencies of immune
451 cells in the placenta and fetal lung, mesenteric fetal lymph node, and fetal blood. Tissues from
452 the placental disc were dissociated into single cell suspensions and assessed for viability using
453 Acridine Orange/Propidium Iodide (Nexcelom Bioscience LLC). Then, samples were stained with
454 a panel of antibodies in Brilliant Stain Buffer (BD Biosciences) for 20 minutes to identify immune
455 cells as previously described.[67] Antibodies used included BD Biosciences: CD3 (SP34-2)-BV650,
456 CD8 (RPA-T8)-BUV395, CD11b (ICRF44)-APC-Cy7, CD11c (SHCL-3)-PE, CD45 (D058-1283)-
457 PE-CF594, CD86 (IT2.2)-PE-Cy5, TCRγδ (B1)-FITC; BioLegend: CD4 (OKT4)-BV605, CD14
458 (M5E2)-BV785, CD16 (3G8)-Alexa Flour 700, CD20 (2H7)-BV570, HLA-DR (L243)-BV711;
459 Invitrogen: CD123 (6H6)-eFlour 450, LIVE/DEAD Fixable Aqua for 405nm excitation; Beckman
460 Coulter: CD159a (Z199)-PC7; and Miltenyi: CD66 (TET2)-APC. The staining protocol proceeded
461 in three steps: LIVE/DEAD Fixable Aqua, then all antibodies other than CD11c and CD123, and
462 finally CD11c and CD123. After staining, samples were fixed with 1% paraformaldehyde and

463 analyzed on a Symphony A3 flow cytometer (BD Biosciences) using FACS Diva 8 software (BD
464 Biosciences). Samples were analyzed using FlowJo 10.9.0 (FlowJo, LLC). All events were initially
465 gated on Forward Scatter (FSC) singlets, CD45+ leukocytes, live cells, and then on FSC-A and
466 Side Scatter (SSC)-A profiles. Populations were defined using canonical markers as described in
467 Table S4. Representative gating strategies are shown for granulocytes (Fig. S8), lymphoid cells
468 (Fig. S9), and monocytes (Fig. S10). Populations were excluded from analysis if they did not meet
469 the minimum threshold of >100 cells in their parent gate.

470

471 *Total RNA-Seq Library Preparation and Analysis*

472 Total RNA sequencing was performed on chorionic villous tissue from the placenta. We used
473 100ng of RNA with RIN>3 as input for RNA library prep using the KAPA RNA HyperPrep kit with
474 RiboErase HMR (#08098131702, Roche Diagnostics Corporation, Indianapolis, IN, USA). The kit
475 was designed for human, mouse, and rat samples, but it also effectively reduced ribosomal RNA
476 in our NHP RNA isolates. Libraries were prepared following the manufacturer's standard protocol.
477 Library quantity and quality were evaluated using Qubit Fluorometer (Thermo Fisher Scientific)
478 and TapeStation (Agilent Technologies, Santa Clara, CA, USA). Constructed libraries were
479 sequenced on a NovaSeq 6000 Sequencing System (#20012850, Illumina, San Diego, CA, USA),
480 which produced 2x100 nucleotide stranded paired-end reads.

481 Raw sequences were aligned to the *Macaca nemestrina* reference genome from Ensembl
482 (Mnem_1.0, INSDC Assembly GCA_000956065.1) utilizing STAR in Partek Flow, a bioinformatics
483 software suite (Partek, Chesterfield, MO, USA). Ensembl gene symbol conversions were
484 employed for consistency across all gene IDs. As the quality score was greater than 35 across all
485 samples, no bases were trimmed, and 100% of sequencing bases overlapped with read lengths
486 of the reference genome. The raw count matrix was downloaded from Partek. Subsequent
487 statistical processing and analysis of count data were performed within the R statistical computing

488 environment (R version 4.4.0). Gene counts were filtered by a row mean of 10 or greater, then
489 normalized using edgeR to implement TMM normalization. Counts were transformed into log2
490 counts using voom, a function in the limma package that modifies RNA-Seq data to create a
491 normalized count matrix.[39,40] Differential Expression (DE) analysis compared placental samples
492 from IAV-infected animals against controls from uninfected animals. Comparisons were based on
493 a linear model fit for each gene using limma. The criteria for all DE analyses included an absolute
494 fold change of 2 and a p-value of less than 0.05. Gene Set Enrichment Analysis was conducted
495 across the comparison group using fgsea with the Broad Institute Molecular Signatures
496 database.[41]

497 Hierarchical clustering analysis, an unsupervised machine learning approach, was performed to
498 group total RNA-Seq profiles based on their similarity in Euclidean distance using the hclust
499 function in R. Ward's linkage was used to minimize variance within each cluster. The optimal
500 number of clusters was determined using the elbow method. The resulting hierarchy was
501 visualized using a dendrogram. Finally, an overrepresentation analysis (ORA) was performed to
502 determine if predefined sets of genes in Gene Ontology (GO) pathways were enriched in the
503 cluster of differentially expressed genes (DEGs) obtained from the hierarchical clustering analysis
504 using the clusterProfiler package in R.

505

506 *Nanostring nCounter®*

507 To validate our results from bulk RNA sequencing, we chose a quantitative multiplex method of
508 direct digital counting of gene transcripts using the Nanostring nCounter® Analysis Systems
509 (Nanostring Technologies Inc., Seattle, WA, USA). RNA extracted from the chorionic villous
510 tissues of the placenta was analyzed using the Nanostring nCounter® NHP Immunology V2 gene
511 expression codeset (#11500276, Nanostring Technologies, Inc). RNA hybridization reactions
512 were performed according to the manufacturer's protocol. Probe-target RNA complexes from all

513 reactions were processed and immobilized on nCounter® cartridges using the nCounter® Prep
514 Station. Gene transcripts were quantified with the nCounter® Digital Analyzer (#MAN-C0035-07,
515 Nanostring Technologies, Inc).

516

517 *Statistical Analyses*

518 All statistical analyses were performed in RStudio (using R version 4.4.0) or nSolver (nCounter
519 data only), both of which use the R programming language. A p-value of less than 0.05 was
520 considered significant, and 0.5-0.1 was reported considering the modest sample size. Groups
521 were compared using non-parametric tests. Spearman's rank correlation coefficient was used to
522 calculate correlations between two variables. Data visualizations were done using ggplot2,
523 ggpmisc, and ComplexHeatmaps packages and their derivatives.[42,43]

524

DATA AVAILABILITY STATEMENT

The data are openly available on several platforms. The metadata, cytokine, RT-qPCR, and flow cytometry are available in the Dryad data repository at https://doi.org/10.5061/dryad.c866t1gjf. The placenta total RNA-Seq data is available through the NIH Gene Expression Omnibus (GEO) via the GSE289117 accession number. Finally, the code used for the computational analysis and to generate the plots is available in GitHub at https://github.com/kadamswaldorflab.

ACKNOWLEDGMENTS

This work was supported by funding from the National Institutes of Health grants R01AI164588 and R01AI176777 to K.A.W.; T32AI007509 to O.C. (PI: Lund); AOA Carolyn Kuckein Student Research Fellowship to M.L.; T32GM007266 to G.M.; and TL1TR002318 to G.M. This work was also supported by the P51OD010425, which is the core grant of the Washington National Primate Research Center. Additional support came from the U42OD011123, which funds the Washington National Primate Research Center breeding colony. The content is solely the responsibility of the authors and does not necessarily represent the official views of the National Institutes of Health.

541 **Table 1. IAV Viral Load in Lung, Placenta, and Clinical Findings**

ID	Clinical Symptoms	Maximum Clinical Score	Maternal Lung Viral Load (copies/mg)	Placenta Viral Load (copies/mg)	Stillbirth
FLU1	Diarrhea: D4, D5	3	2.43×10^6	48.3	No
FLU2	Mild Cough: D4 Dehydration: D5 Moderate Wheezing: D5	3	6.05×10^6	0	No
FLU3	None	0	8.58×10^5	0	No
FLU4	None	0	2.22×10^3	0	No
FLU5	Increased respiratory effort: D2 Mild cough: D3 Not eating: D3, D4	4	2.03×10^6	0	No
FLU6	None	0	5.69×10^5	0	No
FLU7	Decreased appetite: D2	1	2.01×10^4	0	Yes
FLU8	Sneezing: D2, D3 Nasal discharge: D2-D5 Increased respiratory effort: D2-D4 Decreased appetite: D4 Diarrhea: D3, D5	6	1.41×10^6	0	No
FLU9	Nasal discharge: D2, D4 Red nasal discharge: D3, D5 Increased respiratory effort: D2-D5 Decreased appetite: D4 Decreased responsiveness: D5	4	3.17×10^3	64.2	Yes
FLU10	None	0	3.49	0	No
FLU11	Increased respiratory effort: D2, D3 Nasal discharge: D3 Mild coughing: D3	3	8.94×10^5	0	No

542 Clinical symptoms were scored on a 3-point scale with higher scores indicating worse disease
543 and 0 indicating normal. The maximum clinical score was calculated by the sum of the highest
544 recorded scores for each of the 5 clinical areas. Abbreviations: D, day

REFERENCES

1. Chandra, S., Christensen, J., Mamelund, S.E. & Paneth, N. Short-Term Birth Sequelae of the 1918-1920 Influenza Pandemic in the United States: State-Level Analysis. *Am J Epidemiol* **187**, 2585-2595 (2018).
2. Nishiura, H. Excess risk of stillbirth during the 1918-1920 influenza pandemic in Japan. *Eur J Obstet Gynecol Reprod Biol* **147**, 115 (2009).
3. Hardy, J.M., Azarowicz, E.N., Mannini, A., Medearis, D.N., Jr. & Cooke, R.E. The effect of Asian influenza on the outcome of pregnancy, Baltimore, 1957-1958. *Am J Public Health Nations Health* **51**, 1182-1188 (1961).
4. Reid, A. The effects of the 1918-1919 influenza pandemic on infant and child health in Derbyshire. *Med Hist* **49**, 29-54 (2005).
5. Freeman, D.W. & Barno, A. Deaths from Asian influenza associated with pregnancy. *American journal of obstetrics and gynecology* **78**, 1172-1175 (1959).
6. Greenberg, M., Jacobziner, H., Pakter, J. & Weisl, B.A. Maternal mortality in the epidemic of Asian influenza, New York City, 1957. *Am J Obstet Gynecol* **76**, 897-902 (1958).
7. Pierce, M.*, et al.* Perinatal outcomes after maternal 2009/H1N1 infection: national cohort study. *BMJ* **342**, d3214 (2011).
8. Centers for Disease, C. & Prevention. Maternal and infant outcomes among severely ill pregnant and postpartum women with 2009 pandemic influenza A (H1N1)--United States, April 2009-August 2010. *MMWR Morb Mortal Wkly Rep* **60**, 1193-1196 (2011).
9. Haberg, S.E.*, et al.* Risk of fetal death after pandemic influenza virus infection or vaccination. *N Engl J Med* **368**, 333-340 (2013).
10. Rasmussen, S.A., Jamieson, D.J. & Uyeki, T.M. Effects of influenza on pregnant women and infants. *Am J Obstet Gynecol* **207**, S3-8 (2012).
11. Kosmak, G.W. The occurrence of epidemic influenza in pregnancy. *Am J Obstet Gynecol*, 239-251 (1919).
12. Harris, J.W. Influenza Occurring in Pregnant Women: A Statistical Study of Thirteen Hundred and Fifty Cases. *JAMA : the journal of the American Medical Association*, 978-980 (1919).
13. Al-Haddad, B.J.S.*, et al.* The fetal origins of mental illness. *American journal of obstetrics and gynecology* **221**, 549-562 (2019).
14. Barr, C.E., Mednick, S.A. & Munk-Jorgensen, P. Exposure to influenza epidemics during gestation and adult schizophrenia. A 40-year study. *Arch Gen Psychiatry* **47**, 869-874 (1990).
15. Canetta, S.E.*, et al.* Serological documentation of maternal influenza exposure and bipolar disorder in adult offspring. *Am J Psychiatry* **171**, 557-563 (2014).
16. Machon, R.A.*, et al.* Adult schizotypal personality characteristics and prenatal influenza in a Finnish birth cohort. *Schizophr Res* **54**, 7-16 (2002).
17. Machon, R.A., Mednick, S.A. & Huttunen, M.O. Adult major affective disorder after prenatal exposure to an influenza epidemic. *Arch Gen Psychiatry* **54**, 322-328 (1997).
18. Mednick, S.A., Huttunen, M.O. & Machon, R.A. Prenatal influenza infections and adult schizophrenia. *Schizophr Bull* **20**, 263-267 (1994).
19. Mednick, S.A., Machon, R.A., Huttunen, M.O. & Bonett, D. Adult schizophrenia following prenatal exposure to an influenza epidemic. *Arch Gen Psychiatry* **45**, 189-192 (1988).
20. Al-Haddad, B.J.S.*, et al.* Long-term Risk of Neuropsychiatric Disease After Exposure to Infection In Utero. *JAMA Psychiatry* (2019).
21. Regan, A.K.*, et al.* Seasonal Trivalent Influenza Vaccination During Pregnancy and the Incidence of Stillbirth: Population-Based Retrospective Cohort Study. *Clin Infect Dis* **62**, 1221-1227 (2016).

595 22. Bratton, K.N., Wardle, M.T., Orenstein, W.A. & Omer, S.B. Maternal influenza
596 immunization and birth outcomes of stillbirth and spontaneous abortion: a systematic
597 review and meta-analysis. *Clin Infect Dis* **60**, e11-19 (2015).
598 23. Jeong, S., Jang, E.J., Jo, J. & Jang, S. Effects of maternal influenza vaccination on
599 adverse birth outcomes: A systematic review and Bayesian meta-analysis. *PLoS One* **14**,
600 e0220910 (2019).
601 24. Getahun, D.*, et al.* Association between seasonal influenza vaccination with pre- and
602 postnatal outcomes. *Vaccine* **37**, 1785-1791 (2019).
603 25. Giles, M.L., Davey, M.A. & Wallace, E.M. Associations Between Maternal Immunisation
604 and Reduced Rates of Preterm Birth and Stillbirth: A Population Based Retrospective
605 Cohort Study. *Front Immunol* **12**, 704254 (2021).
606 26. Simoes, E.A.F.*, et al.* Trivalent influenza vaccination randomized control trial of pregnant
607 women and adverse fetal outcomes. *Vaccine* **37**, 5397-5403 (2019).
608 27. Influenza in Pregnancy: Prevention and Treatment: ACOG Committee Statement No. 7.
609 *Obstet Gynecol* **143**, e24-e30 (2024).
610 28. Razzaghi, H.*, et al.* Influenza, Tdap, and COVID-19 Vaccination Coverage and Hesitancy
611 Among Pregnant Women - United States, April 2023. *MMWR Morb Mortal Wkly Rep* **72**,
612 1065-1071 (2023).
613 29. Vaccine Confidence Falls as Belief in Health Misinformation Grows. (Annenberg Public
614 Policy Center, University of Pennsylvania, 2023).
615 30. Cunningham, M.C., Maxson A, Mowson R, Pagan D, Garofalini C, Hall K, Bobo M, McCall
616 T.C. 2023 Immunization Profile Study. (National Association of County & City Health
617 Officials, Washington, D.C., 2024).
618 31. Antonson, A.M.*, et al.* Moderately pathogenic maternal influenza A virus infection disrupts
619 placental integrity but spares the fetal brain. *Brain Behav Immun* **96**, 28-39 (2021).
620 32. Van Campen, H.*, et al.* Maternal Influenza A Virus Infection Restricts Fetal and Placental
621 Growth and Adversely Affects the Fetal Thymic Transcriptome. *Viruses* **12**(2020).
622 33. Jacobsen, H.*, et al.* Offspring born to influenza A virus infected pregnant mice have
623 increased susceptibility to viral and bacterial infections in early life. *Nat Commun* **12**, 4957
624 (2021).
625 34. Littauer, E.Q.*, et al.* H1N1 influenza virus infection results in adverse pregnancy outcomes
626 by disrupting tissue-specific hormonal regulation. *PLoS Pathog* **13**, e1006757 (2017).
627 35. Liong, S.*, et al.* Influenza A virus infection during pregnancy causes immunological
628 changes in gut-associated lymphoid tissues of offspring mice. *American journal of*
629 *physiology. Gastrointestinal and liver physiology* **325**, G230-G238 (2023).
630 36. Liong, S.*, et al.* Influenza A virus causes maternal and fetal pathology via innate and
631 adaptive vascular inflammation in mice. *Proc Natl Acad Sci U S A* **117**, 24964-24973
632 (2020).
633 37. Hall, O.J.*, et al.* Progesterone-Based Therapy Protects Against Influenza by Promoting
634 Lung Repair and Recovery in Females. *PLoS Pathog* **12**, e1005840 (2016).
635 38. Vermillion, M.S.*, et al.* Pregnancy preserves pulmonary function following influenza virus
636 infection in C57BL/6 mice. *Am J Physiol Lung Cell Mol Physiol* **315**, L517-l525 (2018).
637 39. Li, M.*, et al.* Non-human Primate Models to Investigate Mechanisms of Infection-
638 Associated Fetal and Pediatric Injury, Teratogenesis and Stillbirth. *Front Genet* **12**(2021).
639 40. Adams Waldorf, K.M., Rubens, C.E. & Gravett, M.G. Use of nonhuman primate models to
640 investigate mechanisms of infection-associated preterm birth. *BJOG* **118**, 136-144 (2011).
641 41. Bouvier, N.M. & Lowen, A.C. Animal Models for Influenza Virus Pathogenesis and
642 Transmission. *Viruses* **2**, 1530-1563 (2010).
643 42. Koday, M.T.*, et al.* Multigenic DNA vaccine induces protective cross-reactive T cell
644 responses against heterologous influenza virus in nonhuman primates. *PloS one* **12**,
645 e0189780 (2017).

646 43. Short, S.J., *et al.* Maternal influenza infection during pregnancy impacts postnatal brain
647 development in the rhesus monkey. *Biol Psychiatry* **67**, 965-973 (2010).
648 44. Mayer, A.E. & Parks, G.D. An AGM model for changes in complement during pregnancy:
649 neutralization of influenza virus by serum is diminished in late third trimester. *PloS one* **9**,
650 e112749 (2014).
651 45. Swieboda, D., *et al.* Pregnancy Downregulates Plasmablast Metabolic Gene Expression
652 Following Influenza Without Altering Long-Term Antibody Function. *Front Immunol* **11**,
653 1785 (2020).
654 46. Garcia-Flores, V., *et al.* Maternal-Fetal Immune Responses in Pregnant Women Infected
655 with SARS-CoV-2. *Res Sq* (2021).
656 47. Brown, A.S., *et al.* Prenatal exposure to maternal infection and executive dysfunction in
657 adult schizophrenia. *Am J Psychiatry* **166**, 683-690 (2009).
658 48. Khandaker, G.M., Zimbron, J., Lewis, G. & Jones, P.B. Prenatal maternal infection,
659 neurodevelopment and adult schizophrenia: a systematic review of population-based
660 studies. *Psychol Med* **43**, 239-257 (2013).
661 49. Kapur, R.P., *et al.* Granular cytoplasmic inclusions in astrocytes and microglial activation
662 in the fetal brain of pigtail macaques in response to maternal viral infection. *Acta*
663 *Neuropathol Commun* **13**, 55 (2025).
664 50. Yawn, D.H., Pyeatte, J.C., Joseph, J.M., Eichler, S.L. & Garcia-Bunuel, R. Transplacental
665 transfer of influenza virus. *JAMA : the journal of the American Medical Association* **216**,
666 1022-1023 (1971).
667 51. McGregor, J.A., Burns, J.C., Levin, M.J., Burlington, B. & Meiklejohn, G. Transplacental
668 passage of influenza A/Bangkok (H3N2) mimicking amniotic fluid infection syndrome. *Am*
669 *J Obstet Gynecol* **149**, 856-859 (1984).
670 52. Davidson, S., Maini, M.K. & Wack, A. Disease-promoting effects of type I interferons in
671 viral, bacterial, and coinfections. *J Interferon Cytokine Res* **35**, 252-264 (2015).
672 53. Barrat, F.J. & Lu, T.T. Role of type I interferons and innate immunity in systemic sclerosis:
673 unbalanced activities on distinct cell types? *Curr Opin Rheumatol* **31**, 569-575 (2019).
674 54. Lawrence, C.W., Ream, R.M. & Braciale, T.J. Frequency, Specificity, and Sites of
675 Expansion of CD8+ T Cells during Primary Pulmonary Influenza Virus Infection1. *The*
676 *Journal of Immunology* **174**, 5332-5340 (2005).
677 55. Kubelkova, K., Bostik, V., Joshi, L. & Macela, A. Innate Immune Recognition, Integrated
678 Stress Response, Infection, and Tumorigenesis. *Biology (Basel)* **12**(2023).
679 56. Wu, Y., Zhang, Z., Li, Y. & Li, Y. The Regulation of Integrated Stress Response Signaling
680 Pathway on Viral Infection and Viral Antagonism. *Front Microbiol* **12**, 814635 (2021).
681 57. Pakos-Zebrucka, K., *et al.* The integrated stress response. *EMBO Rep* **17**, 1374-1395
682 (2016).
683 58. Siston, A.M., *et al.* Pandemic 2009 influenza A(H1N1) virus illness among pregnant
684 women in the United States. *JAMA : the journal of the American Medical Association* **303**,
685 1517-1525 (2010).
686 59. Neuzil, K.M., Reed, G.W., Mitchel, E.F., Simonsen, L. & Griffin, M.R. Impact of influenza
687 on acute cardiopulmonary hospitalizations in pregnant women. *Am J Epidemiol* **148**, 1094-
688 1102 (1998).
689 60. Liu, S., *et al.* Avian influenza virus in pregnancy. *Rev Med Virol* **26**, 268-284 (2016).
690 61. Purcell, R., Giles, M.L., Crawford, N.W. & Buttery, J. Systematic Review of Avian Influenza
691 Virus Infection and Outcomes during Pregnancy. *Emerg Infect Dis* **31**, 50-56 (2025).
692 62. Itoh, Y., *et al.* In vitro and in vivo characterization of new swine-origin H1N1 influenza
693 viruses. *Nature* **460**, 1021-1025 (2009).
694 63. Adams Waldorf, K.M., *et al.* Congenital Zika virus infection as a silent pathology with loss
695 of neurogenic output in the fetal brain. *Nat Med* **24**, 368-374 (2018).

696 64. Boldenow, E., Gendrin, C., Ngo, L., Bierle, C., Vornhagen, J., Coleman, M., Merillat, S.,
697 Armistead, B., Whidbey, C., Alishetti, V., Santana-Ufret,V., Ogle, J., Gough, M.,
698 Srinouanprachanh, S., MacDonald, J., Bammler, T., Bansal, A., Liggitt, H., Rajagopal, L.,
699 Adams Waldorf, K. . Group B Streptococcus circumvents neutrophils and neutrophil
700 extracellular traps during amniotic cavity invasion and preterm labor. *Science Immunology*
701 **1**(2016).
702 65. Reed, L.J. & Muench, H. A simple method of estimating fifty percent endpoints. *Am J Hyg*
703 **27**, 493-497 (1938).
704 66. Yang, Y.*, et al.* Evaluation of Twelve Real-Time Reverse Transcriptase PCR Primer-Probe
705 Sets for Detection of Pandemic Influenza A/H1N1 2009 Virus. *Journal of Clinical*
706 *Microbiology* **49**, 1434-1440 (2011).
707 67. O'Connor, M.A.*, et al.* Early cellular innate immune responses drive Zika viral persistence
708 and tissue tropism in pigtail macaques. *Nat Commun* **9**, 3371 (2018).

709